Large Animal Epilepsy Model Platform: Kainic Acid Porcine Model of Mesial Temporal Lobe Epilepsy

Filip Mivalt[1*×], Daniela Maltais[1*], Inyong Kim[1], Jiwon Kim[1], Patrik Began[1], Andrea Duque Lopez[1], Veronika Krakorova[1], Bailey Winter[1], Nicholas Gregg[1], Daniel Montonye[2], Christopher Gow[2], Kai Miller[3], Jamie Van Gompel[3], Kent Leyde[4], Vaclav Kremen[1,5], Su-youne Chang[1,2†], Gregory A. Worrell[1†×]

[1]Department of Neurology, BNEL (Bioelectronics Neurophysiology & Engineering Lab), Mayo Clinic, Rochester, MN, USA
[2]Department of Comparative Medicine, Mayo Clinic, Rochester, MN, USA
[3]Department of Neurologic Surgery, Mayo Clinic, Rochester, MN, USA
[4]Cadence Neuroscience Inc. Seattle, WA, USA
[5]Czech Institute of Informatics, Robotics, and Cybernetics, Czech Technical University in Prague, Prague, Czech Republic

* Authors contributed equally
× Corresponding authors
† Senior authors: Su-youne Chang and Gregory A. Worrell

Abstract

Translational animal models are essential for advancing neuromodulation therapies for drug-resistant epilepsy. Large animal epilepsy models capable to accommodate implantable neuromodulation devices designed for humans are needed to advance novel neuromodulation therapies. This study aimed to establish and characterize a kainic acid (KA) porcine model of mesial temporal lobe epilepsy (mTLE) as a platform for pre-clinical stimulation therapy development and testing.

We developed a novel platform integrating MRI-guided stereotactic techniques for electrode implantation into bilateral hippocampal (HPC) and anterior nucleus of thalamus (ANT) and intra-hippocampal KA infusion in six domestic pigs. The platform enabled acute intraoperative local field potential (LFP) monitoring in freely behaving animals using a 16-channel fully implantable neural stimulating and recording device designed for human use. Neuropathology was assessed using Cresyl violet staining.

Intra-hippocampal KA infusion successfully induced spontaneous electrophysiological features of mTLE, including interictal epileptiform discharges (IEDs), acute status epilepticus (SE), and seizures. Acute SE occurred in all pigs; four survived chronically. Surviving animals exhibited spontaneous IEDs (4/4) and seizures (3/4), ranging from subclinical events to focal and generalized tonic-clonic seizures. Single pulse evoked potentials confirmed functional ANT-HPC connectivity. Histology showed neuronal loss and disorganization consistent with human mTLE.

The KA-induced porcine mTLE model provides a crucial translational platform uniquely accommodating human-sized neuromodulation devices for testing and validation in freely behaving animals. It enables the development of advanced strategies like automated seizure diaries and closed-loop therapies targeting Papez circuit nodes, directly addressing unmet needs in developing neuromodulation therapies for drug-resistant epilepsy.

Highlights

- We developed a robust large animal model of mTLE using focal hippocampal KA chemotoxin.
- This model provides a pre-clinical platform for both intraoperative and long-term electrophysiological studies in behaving animals using MRI-guided stereotactic techniques and implantable devices designed for humans.
- The porcine KA model replicates hallmarks of human mTLE observed in behaving animals, underscoring its translational potential for evaluating neuromodulation devices and development of novel neuromodulation therapies.

Introduction

Epilepsy is a prevalent neurological disorder affecting approximately 50 million people worldwide (World Health Organization, 2019).-Beyond recurrent seizures, epilepsy is often associated with psychiatric comorbidities including anxiety, depression (Tellez-Zenteno *et al.*, 2007; Bell *et al.*, 2011; Hermann *et al.*, 2021), memory impairments (Bell *et al.*, 2011), cognitive deficits (Bell *et al.*, 2011; Hermann *et al.*, 2021), and sleep disturbances (Bazil, Legros and Kenny, 2003; Khatami *et al.*, 2006; Staniszewska *et al.*, 2017), reflecting complex network pathophysiology (Hermann *et al.*, 2021). These comorbidities are thought to arise from circuit reorganization (Choy *et al.*, 2022), neuroinflammation (Vezzani *et al.*, 2011), neurodegeneration (Reddy and Kuruba, 2013; Zhao *et al.*, 2018), and functional abnormalities (Vrinda *et al.*, 2019). Mesial temporal lobe epilepsy (mTLE) exemplifies challenges of drug-resistant epilepsy and is positioned as a compelling target for development of advanced neuromodulation (Fisher *et al.*, 2010; Morrell and RNS Study Group, 2011; Salanova *et al.*, 2015; Kremen *et al.*, 2018; Nair *et al.*, 2020; Salanova *et al.*, 2021; Denison and Morrell, 2022; Mivalt *et al.*, 2022; Sladky, Kremen, *et al.*, 2022; Sladky, Nejedly, *et al.*, 2022).

Electrical brain stimulation is an established therapy for drug-resistant epilepsy reducing seizure burden with the anterior nucleus of the thalamus (ANT) and hippocampus (HPC) being common neuromodulation targets. However, complete seizure freedom is rare and stimulation parameter optimization is a lengthy process taking months to years because seizures occur sporadically seizure self-reports are highly inaccurate (Fisher *et al.*, 2010; Morrell and RNS Study Group, 2011; Nair *et al.*, 2020; Salanova *et al.*, 2021; Kremen *et al.*, 2025). These challenges motivate the development of the next-generation devices combining sensing and stimulation (Denison and Morrell, 2022; Sladky, Nejedly, *et al.*, 2022).

Developing and testing next-generation neuromodulation devices for epilepsy requires an appropriate animal model that can accommodate human size devices, replicate human physiology, behavior, and therapeutic responses (predictive validity). Rodent models have been extensively used in epilepsy research (Pitkanen, Schwartzkroin and Moshe, 2006). However, rodents are not a suitable translational model for human device testing, due to their small size and limited neuroanatomical complexity. Large animals, such as dogs (Patterson, 2014; Löscher and Worrell, 2022) and pigs (Silfverhuth *et al.*, 2011; Van Gompel *et al.*, 2011; Zhu *et al.*, 2023) provide a gyrencephalic brain structure and sufficient size to support multimodal imaging, surgical procedures, and implantable devices designed for humans.

Chemical induction of seizures with kainic acid (KA) has been widely applied in rodent models (Pitkanen, Schwartzkroin and Moshe, 2006; Lévesque and Avoli, 2013) and recently tested in a porcine model (Zhu *et al.*, 2023). Localized intra-amygdala or intra-hippocampal KA infusion induces pathological features of human hippocampal sclerosis including neuronal cell loss, gliosis, granule cell dispersion, and aberrant mossy fiber sprouting (Blümcke *et al.*, 2007; Kitaura *et al.*, 2018).

Here we develop a porcine mTLE model platform using MRI-guided direct intrahippocampal KA injection with concurrent intra-operative local field potential (LFP) monitoring, advanced neuroimaging protocols, stereotactic electrode placement, video recording and a fully implantable four-lead implantable neural stimulating and recording (INSR) device designed for

human use (Figure 1.). The 4-lead INSR system enables accurate LFP biomarker tracking from multiple nodes of Papez Circuit in freely behaving animals (Martinez-Ramirez *et al.*, 2022).

Additionally, we demonstrate that acute electrophysiology recordings during KA infusion followed by chronic monitoring with a fully implantable INSR device enables the investigation of Papez Circuit connectivity and porcine epilepsy with a direct translational potential to human epilepsy (Fisher *et al.*, 2010; Morrell and RNS Study Group, 2011; Nair *et al.*, 2020; Denison *et al.*, 2021; Salanova *et al.*, 2021; Denison and Morrell, 2022; Sladky, Nejedly, *et al.*, 2022).

Figure 1: A Platform for Development of Chronic Large Animal Epilepsy Models

Methods

This study developed a platform for inducing a porcine model of mTLE using advanced stereotactic techniques. The platform enables acute and chronic LFP monitoring and brain stimulation using a bedside workstation and a fully implantable recording system.

All procedures were conducted under an Institutional Animal Care and Use Committee protocol A00006870 (Mayo Clinic, Rochester, MN.). Six domestic Yorkshire pigs (Sus scrofa; S1-S6; mean weight 17.37 ± 4.34 kg, Table 1) underwent a stereotactic surgery for intra-hippocampal infusion of KA with concurrent LFP monitoring and implant of a fully implantable 4-lead INSR device designed for humans. Electrodes were placed in bilateral ANT and HPC for acute intraoperative and chronic LFP recordings.

Pigs received direct intra-HPC KA injection during intraoperative electrophysiological monitoring. Acute status epilepticus (SE) was induced via stereotactic KA infusion of into the right HPC (see Table 1). Following recovery, animals were housed in temperature-controlled rooms on a 12-hour light/dark cycle, with water provided ad libitum. Enclosure floors were elevated and met established size, material, and sanitation standards (Albus, 2012). Daily enrichment, including treats, chew toys, and human interaction, was provided to promote well-being. All animals were humanely euthanized at the conclusion of the study.

Stereotactic & Recording Instrumentation

The study utilized a custom stereotactic platform for electrode implantation and KA infusion. The stereotactic platform consists of a machined plastic head fixation frame and a modified Leksell arc-frame compatible with a stereotactic targeting software Brainlab (Brainlab AG, Munich, Germany).

A 16-channel Cadence Navia Workstation (Cadence Neuroscience Inc., Seattle, WA) capable of high-fidelity local field potential (LFP) recording (0.1 Hz - 1 kHz bandpass, 8 kHz sampling rate, 24-bit resolution) and programmable stimulation was used for acute intraoperative electrophysiology monitoring.

Chronic LFP monitoring was conducted using a fully implantable, 16-channel Cadence Alera INSR device (Cadence Neuroscience Inc., Seattle, WA). This system records from two digitally selected bipolar derivations at sampling rates of 500 Hz, 2 kHz, or 8 kHz (0.1 Hz - 1 kHz bandpass, 16-bit resolution and a 2 Gbit nonvolatile storage memory). The INSR system includes the implantable device, a programmer, a controller for wireless data transfer via Bluetooth Low Energy, and a charger (Figure 2).

Figure 2 LFP Recording Instrumentation

Pre- and Post-Surgical Imaging

Pre-operative planning was conducted using a 3.0 Tesla MRI (GE Medical Systems). Magnetization-prepared rapid gradient echo (MPRAGE) and fast gray matter acquisition T1 inversion recovery (FGATIR) sequences were selected for their enhanced gray-white matter contrast (Sudhyadhom *et al.*, 2009; Grewal *et al.*, 2018). These MRI sequences, commonly used for electrode lead placement planning in human deep brain stimulation (DBS), provide visualization of critical structures such as the mammillothalamic tract (MTT) for precise direct ANT targeting (Krauss *et al.*, 2021). Post-operative electrode placement was confirmed through computed tomography (CT) (Somatom Flash, Siemens Inc.), co-registered with the pre-operative MRI. Images were analyzed in Brainlab (Brainlab AG, Munich, Germany) and 3D Slicer (Kikinis, Pieper and Vosburgh, 2014) (Figure 3).

Figure 3: Stereotactic Electrode Implantation in the Porcine Model.

Stereotactic Surgery and Kainic Acid Infusion

A custom stereotactic surgery platform consisting of an MRI compatible, machined plastic head fixation frame and a modified Leksell arc-frame (Elekta Inc., Stockholm, Sweden) was used for electrode implantation and KA infusion. Pre-operative MRI scans, combined with stereotactic targeting software (Brainlab AG, Munich, Germany) and porcine brain atlas (Felix *et al.*, 1999), facilitated segmentation and targeting of the bilateral HPC and ANT regions, both common targets in mTLE neuromodulation therapy (Fisher *et al.*, 2010; Morrell and RNS Study Group, 2011; Nair *et al.*, 2020; Salanova *et al.*, 2021; Denison and Morrell, 2022; Sladky, Nejedly, *et al.*, 2022). Four 4-electrode leads were implanted through skull burr holes, secured with "dog-bone" anchors and bone screws. Subjects were maintained under stable isoflurane anesthesia throughout the stereotactic surgery.

Electrodes were connected to the external workstation for acute monitoring using sterile electrode extensions. KA was stereotactically delivered to the hippocampus under combined Ketamine/Xylazine anesthesia using a Hamilton syringe positioned 1-2 mm from the HPC recording electrode contact. KA was administered in 2 μL increments at a rate of 1 μL per minute, with a 10-minute interval between doses. We investigated 16, 6, and 4 μL KA total doses. The KA concentration was 1mg/ml. Seizure activity was terminated using isoflurane 20 minutes after the last KA injection. The isoflurane anesthesia was gradually substituted by a combined Ketamine/Xylazine anesthesia (S5-6) for the duration of KA infusion with a 30-minute isoflurane washout period prior to the KA infusion.

After conclusion of the acute recording, the electrode leads were connected to bifurcation ports of a 2 wire 16-contact extensions tunneled to the implantable neural sensing and recording (INSR) device (Cadence Neuroscience Inc., Seattle, WA) positioned behind the right scapula. Post-surgical CT scans were used to confirm electrode placement.

LFP Recording and Analysis

Cadence Navia workstation was utilized to acutely record LFPs during anesthesia. The workstation was additionally utilized to probe the Papez circuit using single pulse evoked potentials (SPEP). Visual inspection of SPEP with electrical stimulation to ANT and observed evoked potentials in HPC served as a confirmation of correct electrode placement mid-surgery. LFP recording continued also during the KA infusion to confirm electrophysiological seizures.

The LFP recordings were obtained referentially from the ANT and HPC using the 16 electrode contacts (4 contacts on each of the 4 implanted leads). The SPEP were measured as a response to a single pulse stimulation with 6 mA current, 250µs pulse width at 0.1 Hz. The SPEPs were obtained from ANT and HPC at baseline for S5 and S6. A visual review was utilized to intra-operatively identify seizures.

An INSR device implanted behind the right scapula was used for chronic LFP recording with sampling rate of 500 Hz, 2 kHz or 8 kHz. The sampling rate of 500 Hz was utilized to record prolonged LFP recordings (16-24 hours). Higher sampling rates were utilized to record short LFP recordings of 1 minute to 10 minutes periodically. The INSR (Cadence Neuroscience Inc., Seattle, WA, USA) enables stimulation from the 16 contacts and LFP recording from two digitally selected bipolar electrode derivations (Figure 2).

A bipolar LFP channel was derived from the raw acute LFP traces recorded using the Navia workstation for each brain location. The 8 kHz workstation LFPs were subsequently filtered using anti-aliasing filter and down sampled to 500 Hz for further analysis. A narrow band notch filter with quality factor 10 was utilized to suppress 60 Hz powerline noise in the workstation LFP data only. Down sampled workstation LFP data had same sampling rate as the longitudinal INSR LFP traces, and therefore the reminder of the processing is same for the workstation and INSR data.

LFP signals were filtered between 2 Hz and 100 Hz using a finite response (FIR) filter of 101st order. Previously developed Python libraries (Mivalt *et al.*, 2022; Sladky, Nejedly, *et al.*, 2022; Mivalt, Sladky, *et al.*, 2023) were utilized to process LFP signals. Seizures and IEDs were processed using previously validated IED and seizure detectors (Janca *et al.*, 2013; Sladky, Nejedly, *et al.*, 2022).

Histology

The explanted brains were fixed in 4% paraformaldehyde and stored in 30% sucrose in 1X Phosphate-Buffered Saline. Brains were frozen with dry ice and cut to 60-µm thick coronal sections on a sliding microtome (Leica Biosystems, Wetzlar, Germany) in serial order starting from the corpus callosum anteriorly to the caudal end of the ventral hippocampus. Brain sections were immersed in a 1% CV acetate solution (Sigma-Aldrich, C5042) for approximately 5 minutes. Subsequently, the slides were immersed in 70% EtOH for 10 minutes. Further removal

of excess stain was achieved by immersing the sections in 95% EtOH with 150 uL of acetic acid for approximately 3 minutes, followed by two series of 5-minute baths of 100% EtOH and xylene. Finally, the slices were cover slipped using Eukitt® Quick-hardening mounting medium (03989, Sigma-Aldrich), and imaged under a microscope (Keyence, BZ-X800). The protocol was inspired by (Pilati *et al.*, 2008; Kang, Watanabe and Shen, 2021; Liu *et al.*, 2021) Slides were visually examined for differences between the control and the KA injected CA1, CA3 and dentate gyrus regions using available pig brain atlases. (Felix *et al.*, 1999; Bjarkam *et al.*, 2017).

Results

We developed a porcine mTLE model using stereotactic intrahippocampal KA injection. Both intra-operative and chronic electrophysiology were collected and analyzed. The pre-op imaging, stereotactic targeting, intra-op recording, and chronic recordings in freely behaving animals were developed with systems designed for human epilepsy.

Acute and Chronic Electrophysiology Monitoring

We monitored acute and chronic electrophysiological changes to assess SE duration, interictal epileptiform discharges, and spontaneous seizures. SE was observed in all animals following 16, 6, and 4 µl KA infusion into unilateral hippocampus. Two pigs (S1 & S6) were euthanized within the first 12 hours of recovery due to uncontrolled SE and cardiopulmonary arrest.

The initial pig (S1) received 16µl KA and was euthanized because the acute SE could not be aborted. One of the four pigs (S6) receiving 6 µL KA dosing was euthanized after a cardiopulmonary arrest during recovery.

Of the remaining surviving four animals, 100% (4/4) exhibited spontaneous IEDs, and 75% (3/4) displayed spontaneous seizures during the chronic phase, with initial focal HPC seizures occurring an average of 10.33 ± 3.40 days post-KA infusion.

Table 1 near here: Summary of Animal Outcomes and Electrophysiology.

Papez Circuit Electrophysiology

Sixteen channels of local field potentials (LFPs) were recorded intraoperatively, with four channels from each ANT and HPC electrode under anesthesia. Baseline recordings were obtained prior to KA infusion, along with single pulse evoked potentials (SPEP) in two pigs, enabling assessment of ANT-HPC connectivity.

Baseline LFPs showed lower amplitudes and power spectral density in the ANT compared to the HPC (ANT: 0.80 ± 3.92 µV/Hz vs HPC: 8.77 ± 5.83 µV/Hz; $p < 10^{-6}$, Mann-Whitney U-test), consistent with human recordings (Mivalt *et al.*, 2022). Following KA infusion, LFPs exhibited increased spectral power, and seizure activity (Figure 4.). SPEP asymmetries between ANT and HPC suggest latency and amplitude differences, highlighting functional circuit properties (ANT → HPC latency vs HPC → ANT latency: 16.64 ± 5.88 ms vs. 8.44 ± 2.25 ms, $p < 0.0001$, Mann-Whitney U-test) (Figure 4). The significantly larger magnitude for the HPC → HPC SPEP than ANT →HPC (1.81 ± 0.23 µV vs 2.41±0.25 µV, U = 965.0, $p < 0.0001$, Mann Whitney U-test)

suggests a very strong connectivity between bilateral HPC structures in a swine brain (Figure 4). We did not perform SPEP recordings post-KA.

Figure 4 Intraoperative Electrophysiology of Papez Circuit and Acute Status Epilepticus

Kainic Acid (KA) Infusion and Acute Seizure Dynamics
KA infusion into the HPC elicited a marked increase in LFP amplitude, accompanied by the onset of IEDs and seizures. Initial focal seizure was localized to the injection site (Figure 4.). Pathological activity subsequently spread to contralateral HPC and ANT, demonstrating seizure propagation. During the intra-operative period breakthrough clinical seizures, characterized by increased heart rate and mild tremors, emerged despite deep anesthesia. Intraoperative clinical seizures were controlled in some cases by increasing isoflurane doses to achieve a burst suppression pattern. After approximately 20 minutes of SE, isoflurane and intravenous benzodiazepines were used to terminate SE.

Upon emergence from anesthesia, bilateral hippocampal seizure activity persisted and occasionally progressed to focal to bilateral tonic-clonic seizures (FBTCS). These seizures included tonic extension of the left forelimb, lateral head deviation, and generalized clonic movements. Limb movements resembling "running" were also intermittently observed. Seizure activity persisted for over an hour post-operatively and was corroborated by LFP seizure patterns in the HPC.

Subjects S1 and S6 were euthanized within 12 hours of surgery. Subject S1 received 16 µl KA injection followed by refractory SE that was unresponsive to intravenous diazepam. Continued LFP seizures were recorded by the INSR device and the animal euthanized. Subject S6 received 6 µl KA and had a prolonged seizures post-operatively and received diazepam (1 mg/kg). The pig experienced cardiopulmonary arrest, and resuscitation was unsuccessful. Autopsy revealed cardiac pathology, including dilated ventricles with thin walls, possibly contributing to cardiopulmonary arrest and death. S3 and S4 were euthanized on day 10 and 19 after the implant surgery due to developed infection in the wound around the INSR device.

Seizures and IED during chronic monitoring in behaving pig mTLE model
The four surviving chronic pigs were maintained and monitored using video and the INSR device for a total of 86.25 ± 107.44 days (Table 1.). Interictal epileptiform discharges (IEDs) were observed in all four subjects. The IEDs showed multiple morphologies including spike and wave discharges, high frequency oscillations, delta brush LFP waveforms- all of which have been reported in previous KA seizure models (Bragin *et al.*, 1999; Lévesque and Avoli, 2013; Zhu *et al.*, 2023) (Figure 5).

We observed independent and synchronous spontaneous IEDs, but with higher hourly IED rate in the right HPC (KA site) compared to the left HPC (right 352.68 ± 338.49 vs. left 174.59 ± 269.71, $p < 0.0001$, Mann Whitney U-test) in all four subjects.

A total of 2,733 (683.25 ± 694.82) electrographic seizures were recorded over 386 days (96.5 ± 104.94) (Table 1). The average seizure duration was 27.16±17.62 seconds and we recorded in average 32.37 ± 43.67 seizures per day (Table 1). We observed multiple behavioral seizure

correlates including generalized tonic clonic convulsive seizures, myoclonic jerks, absence HPC seizures with impaired consciousness consisted of a sudden cessation of activity and lack of responsiveness to external stimuli with LFP seizure propagating from right HPC to left

Figure 5. Spontaneous Interictal Epileptiform Discharges (IED) and Seizures in Chronic Pig Model.

Histology

We used visual review of cresyl violet staining to qualitatively characterize the histopathologic changes of HPC after KA injections. The animals were euthanized after 1 – 6 months. We observed disorganization, dispersion and non-specific patches of pyramidal cell loss predominantly in the lesioned CA3 ventral hippocampal region, compared to the contralateral control. Both ventral hippocampal CA1 regions had extensive pyramidal cell dispersion. However, the KA-injected side also exhibited non-specific patches of pyramidal cell loss alongside shrinkage in the size of the large pyramidal cells and the presence of dark pyknotic nuclei among the remaining cells. Previous literature has qualitatively described the pathological patterns of distribution of the granular cells within the dentate gyrus as normal, neuronal cell loss, dispersion, and bilamination. Granular cell dispersion and minimal granular cell loss were observed in the dentate gyrus region of the lesioned HPC (Jardim *et al.*, 2021). There was evidence of pyknotic nuclei amongst the granular cells. Overall, cresyl violet staining revealed a significant number of pyknotic pyramidal cells and significant cell loss in CA1 and CA3 regions (Figure 6).

Figure 6. Histology samples of the lesioned vs control HPC.

Discussion

In this study, we developed a system for induction of porcine mTLE and chronic LFP monitoring using a fully implantable INSR system targeting multiple nodes of limbic circuit. The image-guided stereotactic KA infusion for targeted lesioning induced acute SE and subsequent epilepsy characterized by spontaneous IEDs and seizures. This model demonstrates key pathological and electrophysiological features of human mTLE, making it a promising platform for translational research and development of the next-generation neuromodulation devices and therapies. Large animal models of epilepsy represent a vital step in the development and testing of implantable technologies designed for human use.

Additionally, the developed platform utilizing advanced imaging protocols, accurate stereotactic drug infusion, and chronic LFP monitoring in freely behaving animals can be utilized for development of disease models beyond mTLE. Similarly, the presented KA mTLE model induction protocol can be utilized for testing of different neuromodulation systems and therapies beyond herein utilized instrumentation.

Survival and Seizure Outcomes (Table 1) The pigs received either 16µl (1/6), 6µl (4/6), or 4µl (1/6) intra-hippocampal KA to optimize the balance between inducing mTLE and mortality. Four out of six animals (66%) survived the acute SE phase. All surviving pigs exhibited spontaneous IEDs, with three developing spontaneous HPC seizures and mTLE supporting the model's utility. These results are consistent with a prior intra-hippocampal KA study in pigs (Zhu *et al.*, 2023). Our data shows that 4µl induced IEDs but not chronic seizures in S4, while 6µl induced seizures but had associated mortality/morbidity, suggesting an optimal dose might be between 4-6µl however this requires further refinement and larger cohort studies.

Implications for Neuromodulation Device Development The porcine mTLE model provides a unique opportunity to advance neuromodulation therapies. The relatively large brain size and ability to accommodate electrode leads and INSR devices designed for humans will be useful for testing neuromodulation and sensing paradigms (Mivalt *et al.*, 2022; Sladky, Kremen, *et al.*, 2022; Sladky, Nejedly, *et al.*, 2022; Mivalt, Kremen, *et al.*, 2023; Ayyoubi *et al.*, 2024).

Characterization of the Papez Circuit We assessed connectivity within the Papez circuit (ANT ↔ HPC) using single pulse evoked potentials, demonstrating functional connectivity between ANT and HPC. This approach quantifies the circuit properties and offers a potential biomarker for tracking neural state changes, such as those related to sleep-wake cycles (Mivalt *et al.*, 2022) and seizure susceptibility (Lepeu *et al.*, 2024). Moreover, porcine Papez Circuit SPEPs exhibit similarities with humans (Štillová *et al.*, 2015; Wang *et al.*, 2020; Ojeda Valencia *et al.*, 2023). Further investigation into Papez circuit neuromodulation could prove useful for understanding memory, mood, and sleep epilepsy comorbidities (Balzekas *et al.*, 2021; Mivalt *et al.*, 2022; Kremen *et al.*, 2024).

Limitations and Future Directions This study is limited by the small sample size, which may affect the generalizability of findings. Additionally, we were unable to assess post-KA SPEP changes due to logistical limitations, leaving a gap in understanding the effect of KA on evoked responses. Future studies should include a larger cohort to validate findings and refine KA dosing for improved survival and chronic seizure outcomes. Lastly, incorporating behavioral

assessments, such as memory, mood, and sleep alongside electrophysiological monitoring would enhance our understanding of seizure-related comorbidities in this model (Balzekas *et al.*, 2021; Mivalt, Sladky, *et al.*, 2023). Finally, exploring additional neuromodulation targets within the Papez circuit could provide insights into broader therapeutic applications for epilepsy-related cognitive and emotional deficits.

Conclusion

We successfully demonstrated a pig model of mTLE, providing a platform for the pre-clinical development and testing of next-generation implantable devices designed for humans. This model demonstrates reliable induction of chronic epilepsy through targeted hippocampal KA injections, with spontaneous IEDs and seizures observed in surviving animals. The model supports chronic monitoring in freely behaving animals and testing of novel sensing and stimulation paradigms, making it suitable for developing seizure detection algorithms and closed-loop neuromodulation therapies. Our findings underscore the translational potential of a porcine mTLE model for addressing unmet clinical needs of novel stimulation therapies in drug-resistant epilepsy.

Acknowledgement

This research was supported by NIH R01-NS092882, Birdel Fund Mayo Clinic Philanthropy and Cadence Neuroscience who provided the electrophysiology neural workstation and the INSR devices. We thank the XRI Core and Department of Comparative Medicine within Mayo Clinic for supporting our experiments.

Conflict of Interest

G.A.W., J.V.G are named inventors for intellectual property developed at Mayo Clinic and licensed to Cadence Neuroscience. G.A.W. has licensed intellectual property developed at Mayo Clinic to NeuroOne. Mayo Clinic has received research support and consulting fees on behalf of G.A.W. from Cadence Neuroscience, UNEEG Medical, NeuroOne, Epiminder, Medtronic, and Philips Neuro. F.M. has received a salary support from Cadence Neuroscience Inc.

References

Albus, U. (2012) “Guide for the Care and Use of Laboratory Animals (8th edn),” *Laboratory animals*, 46(3), pp. 267–268. Available at: https://doi.org/10.1258/la.2012.150312.

Ayyoubi, A.H., Besheli, B.F., Quach, M.M., Gavvala, J.R., Goldman, A.M., Swamy, C.P., Bartoli, E., Curry, D.J., Sheth, S.A., Francis, D.J. and Ince, N. (2024) “Benchmarking signal quality and spatiotemporal distribution of interictal spikes in prolonged human iEEG recordings

using CorTec wireless brain interchange," *Scientific reports*, 14. Available at: https://doi.org/10.1038/s41598-024-52487-5.

Balzekas, I., Sladky, V., Nejedly, P., Brinkmann, B.H., Crepeau, D., Mivalt, F., Gregg, N.M., Pal Attia, T., Marks, V.S., Wheeler, L., Riccelli, T.E., Staab, J.P., Lundstrom, B.N., Miller, K.J., Van Gompel, J., Kremen, V., Croarkin, P.E. and Worrell, G.A. (2021) "Invasive Electrophysiology for Circuit Discovery and Study of Comorbid Psychiatric Disorders in Patients With Epilepsy: Challenges, Opportunities, and Novel Technologies," *Frontiers in human neuroscience*, 15, p. 702605. Available at: https://doi.org/10.3389/fnhum.2021.702605.

Bazil, C.W., Legros, B. and Kenny, E. (2003) "Sleep structure in patients with psychogenic nonepileptic seizures," *Epilepsy & behavior: E&B*, 4(4), pp. 395–398. Available at: https://doi.org/10.1016/s1525-5050(03)00120-3.

Bell, B., Lin, J.J., Seidenberg, M. and Hermann, B. (2011) "The neurobiology of cognitive disorders in temporal lobe epilepsy," *Nature reviews. Neurology*, 7(3), pp. 154–164. Available at: https://doi.org/10.1038/nrneurol.2011.3.

Bjarkam, C.R., Glud, A.N., Orlowski, D., Sørensen, J.C.H. and Palomero-Gallagher, N. (2017) "The telencephalon of the Göttingen minipig, cytoarchitecture and cortical surface anatomy," *Brain structure & function*, 222(5), pp. 2093–2114. Available at: https://doi.org/10.1007/s00429-016-1327-5.

Blümcke, I., Pauli, E., Clusmann, H., Schramm, J., Becker, A., Elger, C., Merschhemke, M., Meencke, H.-J., Lehmann, T., von Deimling, A., Scheiwe, C., Zentner, J., Volk, B., Romstöck, J., Stefan, H. and Hildebrandt, M. (2007) "A new clinico-pathological classification system for mesial temporal sclerosis," *Acta neuropathologica*, 113(3), pp. 235–244. Available at: https://doi.org/10.1007/s00401-006-0187-0.

Bragin, A., Engel, J., Jr, Wilson, C.L., Vizentin, E. and Mathern, G.W. (1999) "Electrophysiologic analysis of a chronic seizure model after unilateral hippocampal KA injection," *Epilepsia*, 40(9), pp. 1210–21.

Choy, M., Dadgar-Kiani, E., Cron, G.O., Duffy, B.A., Schmid, F., Edelman, B.J., Asaad, M., Chan, R.W., Vahdat, S. and Lee, J.H. (2022) "Repeated hippocampal seizures lead to brain-wide reorganization of circuits and seizure propagation pathways," *Neuron*, 110(2), pp. 221-236.e4. Available at: https://doi.org/10.1016/j.neuron.2021.10.010.

Denison, T., Koubeissi, M., Krook-Magnuson, E., Mogul, D., Worrell, G. and Schevon, C. (2021) "Stimulating Solutions for Intractable Epilepsy," *Epilepsy currents*, 21(5), p. 15357597211012466. Available at: https://doi.org/10.1177/15357597211012466.

Denison, T. and Morrell, M.J. (2022) "Neuromodulation in 2035: The neurology future forecasting series," *Neurology*, 98(2), pp. 65–72. Available at: https://doi.org/10.1212/WNL.0000000000013061.

Felix, B., Leger, M.E., Albe-Fessard, D., Marcilloux, J.C., Rampin, O. and Laplace, J.P. (1999) "Stereotaxic atlas of the pig brain," *Brain research bulletin*, 49(1–2), pp. 1–137. Available at: https://doi.org/10.1016/s0361-9230(99)00012-x.

Fisher, R., Salanova, V., Witt, T., Worth, R., Henry, T., Gross, R., Oommen, K., Osorio, I., Nazzaro, J., Labar, D., Kaplitt, M., Sperling, M., Sandok, E., Neal, J., Handforth, A., Stern, J., DeSalles, A., Chung, S., Shetter, A., Bergen, D., Bakay, R., Henderson, J., French, J., Baltuch, G., Rosenfeld, W., Youkilis, A., Marks, W., Garcia, P., Barbaro, N., Fountain, N., Bazil, C., Goodman, R., McKhann, G., Babu Krishnamurthy, K., Papavassiliou, S., Epstein, C., Pollard, J., Tonder, L., Grebin, J., Coffey, R., Graves, N. and SANTE Study Group (2010) "Electrical stimulation of the anterior nucleus of thalamus for treatment of refractory epilepsy: Deep Brain Stimulation of Anterior Thalamus for Epilepsy," *Epilepsia*, 51(5), pp. 899–908. Available at: https://doi.org/10.1111/j.1528-1167.2010.02536.x.

Grewal, S.S., Middlebrooks, E.H., Kaufmann, T.J., Stead, M., Lundstrom, B.N., Worrell, G.A., Lin, C., Baydin, S. and Van Gompel, J.J. (2018) "Fast gray matter acquisition T1 inversion recovery MRI to delineate the mammillothalamic tract for preoperative direct targeting of the anterior nucleus of the thalamus for deep brain stimulation in epilepsy," *Neurosurgical focus*, 45(2), p. E6. Available at: https://doi.org/10.3171/2018.4.FOCUS18147.

Hermann, B.P., Struck, A.F., Dabbs, K., Seidenberg, M. and Jones, J.E. (2021) "Behavioral phenotypes of temporal lobe epilepsy," *Epilepsia open*, 6(2), pp. 369–380. Available at: https://doi.org/10.1002/epi4.12488.

Janca, R., Jezdik, P., Cmejla, R., Krsek, P., Jefferys, J.G.R., Marusic, P. and Jiruska, P. (2013) *Automatic detection and spatial clustering of interictal discharges in invasive recordings*. (MeMeA 2013 - IEEE International Symposium on Medical Measurements and Applications, Proceedings). Available at: https://doi.org/10.1109/MeMeA.2013.6549739.

Jardim, A.P., Duarte, J.T.C., Lancellotti, C.L.P., Carrete, H., Jr, Centeno, R.S., Scorza, C.A., Cavalheiro, E.A., Guaranha, M.S.B. and Yacubian, E.M.T. (2021) "Granule cell dispersion is associated with hippocampal neuronal cell loss, initial precipitating injury, and other clinical features in mesial temporal lobe epilepsy and hippocampal sclerosis," *Seizure: the journal of the British Epilepsy Association*, 90, pp. 60–66. Available at: https://doi.org/10.1016/j.seizure.2021.05.024.

Kang, J., Watanabe, H. and Shen, J. (2021) "Protocols for assessing neurodegenerative phenotypes in Alzheimer's mouse models," *STAR protocols*, 2(3), p. 100654. Available at: https://doi.org/10.1016/j.xpro.2021.100654.

Khatami, R., Zutter, D., Siegel, A., Mathis, J., Donati, F. and Bassetti, C.L. (2006) "Sleep-wake habits and disorders in a series of 100 adult epilepsy patients--a prospective study," *Seizure: the journal of the British Epilepsy Association*, 15(5), pp. 299–306. Available at: https://doi.org/10.1016/j.seizure.2006.02.018.

Kikinis, R., Pieper, S.D. and Vosburgh, K.G. (2014) "3D slicer: A platform for subject-specific image analysis, visualization, and clinical support," in *Intraoperative Imaging and Image-*

Guided Therapy. New York, NY: Springer New York, pp. 277–289. Available at: https://doi.org/10.1007/978-1-4614-7657-3_19.

Kitaura, H., Shirozu, H., Masuda, H., Fukuda, M., Fujii, Y. and Kakita, A. (2018) "Pathophysiological characteristics associated with epileptogenesis in human hippocampal sclerosis," *EBioMedicine*, 29, pp. 38–46. Available at: https://doi.org/10.1016/j.ebiom.2018.02.013.

Krauss, J.K., Lipsman, N., Aziz, T., Boutet, A., Brown, P., Chang, J.W., Davidson, B., Grill, W.M., Hariz, M.I., Horn, A., Schulder, M., Mammis, A., Tass, P.A., Volkmann, J. and Lozano, A.M. (2021) "Technology of deep brain stimulation: current status and future directions," *Nature reviews. Neurology*, 17(2), pp. 75–87. Available at: https://doi.org/10.1038/s41582-020-00426-z.

Kremen, V., Brinkmann, B.H., Kim, I., Guragain, H., Nasseri, M., Magee, A.L., Attia, T.P., Nejedly, P., Sladky, V., Nelson, N., Chang, S.Y., Herron, J.A., Adamski, T., Baldassano, S., Cimbalnik, J., Vasoli, V., Fehrmann, E., Chouinard, T., Patterson, E.E., Litt, B., Stead, M., Van Gompel, J., Sturges, B.K., Jo, H.J., Crowe, C.M., Denison, T. and Worrell, G.A. (2018) "Integrating brain implants with local and distributed computing devices: A next generation epilepsy management system," *IEEE journal of translational engineering in health and medicine*, 6. Available at: https://doi.org/10.1109/JTEHM.2018.2869398.

Kremen, V., Sladky, V., Mivalt, F., Gregg, N., Brinkmann, B., Balzekas, I., Marks, V., Kucewicz, M., Lundstrom, B., Cui, J., St. Louis, E., Croarkin, P.E., Alden, E.C., Joseph, B., Fields, J., Crockett, K., Adolf, J., Bilderbeek, J.A., Hermes, D., Messina, S., Miller, K., Van Gompel, J.J., Denison, T. and Worrell, G. (2025) "Modulating limbic circuits in temporal lobe epilepsy: impacts on seizures, memory, mood and sleep," *Brain communications*, 7(2), p. fcaf106. Available at: https://doi.org/10.1093/braincomms/fcaf106.

Kremen, V., Sladky, V., Mivalt, F., Gregg, N.M., Balzekas, I.M., Marks, T., Brinkmann, B.H., Lundstrom, B.N., Cui, R., Louis, E.K.S., Croarkin, P., Alden, E., Fields, J., Crockett, K., Adolf, J., Bilderbeek, J., Miller, D.H., Messina, S., Miller, K.J., Van Gompel, J., Denison, T. and Worrell, G.A. (2024) "Platform for brain network sensing and stimulation with quantitative behavioral tracking: Application to limbic circuit epilepsy." medRxiv. Available at: https://doi.org/10.1101/2024.02.09.24302358.

Lepeu, G., van Maren, E., Slabeva, K., Friedrichs-Maeder, C., Fuchs, M., Z'Graggen, W.J., Pollo, C., Schindler, K.A., Adamantidis, A., Proix, T. and Baud, M.O. (2024) "The critical dynamics of hippocampal seizures," *Nature communications*, 15(1), p. 6945. Available at: https://doi.org/10.1038/s41467-024-50504-9.

Lévesque, M. and Avoli, M. (2013) "The kainic acid model of temporal lobe epilepsy," *Neuroscience and biobehavioral reviews*, 37(10 Pt 2), pp. 2887–2899. Available at: https://doi.org/10.1016/j.neubiorev.2013.10.011.

Liu, Y., Bergmann, T., Mori, Y., Peralvo Vidal, J.M., Pihl, M., Vasistha, N.A., Thomsen, P.D., Seemann, S.E., Gorodkin, J., Hyttel, P., Khodosevich, K., Witter, M.P. and Hall, V.J. (2021) "Development of the entorhinal cortex occurs via parallel lamination during neurogenesis,"

Frontiers in neuroanatomy, 15, p. 663667. Available at: https://doi.org/10.3389/fnana.2021.663667.

Löscher, W. and Worrell, G.A. (2022) "Novel subscalp and intracranial devices to wirelessly record and analyze continuous EEG in unsedated, behaving dogs in their natural environments: A new paradigm in canine epilepsy research," *Frontiers in veterinary science*, 9, p. 1014269. Available at: https://doi.org/10.3389/fvets.2022.1014269.

Martinez-Ramirez, L., Slate, A., Price, G., Duhaime, A.-C., Staley, K. and Costine-Bartell, B.A. (2022) "Robust, long-term video EEG monitoring in a porcine model of post-traumatic epilepsy," *eNeuro*, 9(4), p. ENEURO.0025-22.2022. Available at: https://doi.org/10.1523/ENEURO.0025-22.2022.

Mivalt, F., Kremen, V., Sladky, V., Balzekas, I., Nejedly, P., Gregg, N.M., Lundstrom, B.N., Lepkova, K., Pridalova, T., Brinkmann, B.H., Jurak, P., Van Gompel, J.J., Miller, K., Denison, T., St Louis, E.K. and Worrell, G.A. (2022) "Electrical brain stimulation and continuous behavioral state tracking in ambulatory humans," *Journal of neural engineering*, 19(1), p. 016019. Available at: https://doi.org/10.1088/1741-2552/ac4bfd.

Mivalt, F., Kremen, V., Sladky, V., Cui, J., Gregg, N.M., Balzekas, I., Marks, V., St Louis, E.K., Croarkin, P., Lundstrom, B.N., Nelson, N., Kim, J., Hermes, D., Messina, S., Worrell, S., Richner, T., Brinkmann, B.H., Denison, T., Miller, K.J., Van Gompel, J., Stead, M. and Worrell, G.A. (2023) "Impedance rhythms in human limbic system," *The Journal of neuroscience: the official journal of the Society for Neuroscience*, 43(39), pp. 6653–6666. Available at: https://doi.org/10.1523/JNEUROSCI.0241-23.2023.

Mivalt, F., Sladky, V., Worrell, S., Gregg, N.M., Balzekas, I., Kim, I., Chang, S.-Y., Montonye, D.R., Duque-Lopez, A., Krakorova, M., Pridalova, T., Lepkova, K., Brinkmann, B.H., Miller, K.J., Van Gompel, J.J., Denison, T., Kaufmann, T.J., Messina, S.A., St Louis, E.K., Kremen, V. and Worrell, G.A. (2023) "Automated sleep classification with chronic neural implants in freely behaving canines," *Journal of neural engineering*, 20(4). Available at: https://doi.org/10.1088/1741-2552/aced21.

Morrell, M.J. and RNS Study Group (2011) "Responsive cortical stimulation for the treatment of medically intractable partial epilepsy," *Neurology*, 77(13), pp. 1295–1304. Available at: https://doi.org/10.1212/WNL.0b013e3182302056.

Nair, D.R., Laxer, K.D., Weber, P.B., Murro, A.M., Park, Y.D., Barkley, G.L., Smith, B.J., Gwinn, R.P., Doherty, M.J., Noe, K.H., Zimmerman, R.S., Bergey, G.K., Anderson, W.S., Heck, C., Liu, C.Y., Lee, R.W., Sadler, T., Duckrow, R.B., Hirsch, L.J., Wharen, R.E., Jr, Tatum, W., Srinivasan, S., McKhann, G.M., Agostini, M.A., Alexopoulos, A.V., Jobst, B.C., Roberts, D.W., Salanova, V., Witt, T.C., Cash, S.S., Cole, A.J., Worrell, G.A., Lundstrom, B.N., Edwards, J.C., Halford, J.J., Spencer, D.C., Ernst, L., Skidmore, C.T., Sperling, M.R., Miller, I., Geller, E.B., Berg, M.J., Fessler, A.J., Rutecki, P., Goldman, A.M., Mizrahi, E.M., Gross, R.E., Shields, D.C., Schwartz, T.H., Labar, D.R., Fountain, N.B., Elias, W.J., Olejniczak, P.W., Villemarette-Pittman, N.R., Eisenschenk, S., Roper, S.N., Boggs, J.G., Courtney, T.A., Sun, F.T., Seale, C.G., Miller, K.L., Skarpaas, T.L., Morrell, M.J. and RNS System LTT Study (2020) "Nine-year

prospective efficacy and safety of brain-responsive neurostimulation for focal epilepsy," *Neurology*, 95(9), pp. e1244–e1256. Available at: https://doi.org/10.1212/WNL.0000000000010154.

Ojeda Valencia, G., Gregg, N.M., Huang, H., Lundstrom, B.N., Brinkmann, B.H., Pal Attia, T., Van Gompel, J.J., Bernstein, M.A., In, M.-H., Huston, J., 3rd, Worrell, G.A., Miller, K.J. and Hermes, D. (2023) "Signatures of electrical stimulation driven network interactions in the human limbic system," *The Journal of neuroscience: the official journal of the Society for Neuroscience*, 43(39), pp. 6697–6711. Available at: https://doi.org/10.1523/JNEUROSCI.2201-22.2023.

Patterson, E.E. (2014) "Canine epilepsy: an underutilized model," *ILAR journal*, 55(1), pp. 182–186. Available at: https://doi.org/10.1093/ilar/ilu021.

Pilati, N., Barker, M., Panteleimonitis, S., Donga, R. and Hamann, M. (2008) "A rapid method combining Golgi and Nissl staining to study neuronal morphology and cytoarchitecture," *The journal of histochemistry and cytochemistry: official journal of the Histochemistry Society*, 56(6), pp. 539–550. Available at: https://doi.org/10.1369/jhc.2008.950246.

Pitkanen, A., Schwartzkroin, P.A. and Moshe, S.L. (2006) *Models of seizures and epilepsy*. London, England: Academic Press Inc. (London).

Reddy, D.S. and Kuruba, R. (2013) "Experimental models of status epilepticus and neuronal injury for evaluation of therapeutic interventions," *International journal of molecular sciences*, 14(9), pp. 18284–18318. Available at: https://doi.org/10.3390/ijms140918284.

Salanova, V., Sperling, M.R., Gross, R.E., Irwin, C.P., Vollhaber, J.A., Giftakis, J.E., Fisher, R.S. and SANTÉ Study Group (2021) "The SANTÉ study at 10 years of follow-up: Effectiveness, safety, and sudden unexpected death in epilepsy," *Epilepsia*, 62(6), pp. 1306–1317. Available at: https://doi.org/10.1111/epi.16895.

Salanova, V., Witt, T., Worth, R., Henry, T.R., Gross, R.E., Nazzaro, J.M., Labar, D., Sperling, M.R., Sharan, A., Sandok, E., Handforth, A., Stern, J.M., Chung, S., Henderson, J.M., French, J., Baltuch, G., Rosenfeld, W.E., Garcia, P., Barbaro, N.M., Fountain, N.B., Elias, W.J., Goodman, R.R., Pollard, J.R., Tröster, A.I., Irwin, C.P., Lambrecht, K., Graves, N., Fisher, R. and SANTE Study Group (2015) "Long-term efficacy and safety of thalamic stimulation for drug-resistant partial epilepsy," *Neurology*, 84(10), pp. 1017–1025. Available at: https://doi.org/10.1212/WNL.0000000000001334.

Silfverhuth, M.J., Kortelainen, J., Ruohonen, J., Suominen, K., Niinimäki, J., Sonkajärvi, E., Kiviniemi, V., Alahuhta, S., Jäntti, V., Tervonen, O. and Seppänen, T. (2011) "A characteristic time sequence of epileptic activity in EEG during dynamic penicillin-induced focal epilepsy--a preliminary study," *Seizure: the journal of the British Epilepsy Association*, 20(7), pp. 513–519. Available at: https://doi.org/10.1016/j.seizure.2011.03.006.

Sladky, V., Kremen, V., McQuown, K., Mivalt, F., Brinkmann, B.H., Van Gompel, J., Miller, K.J., Denison, T. and Worrell, G.A. (2022) "Integrated human-machine interface for closed-loop stimulation using implanted and wearable devices," in. *2022 IEEE International Conference on*

Systems, Man, and Cybernetics (SMC), pp. 1730–1735. Available at: https://doi.org/10.1109/smc53654.2022.9945203.

Sladky, V., Nejedly, P., Mivalt, F., Brinkmann, B.H., Kim, I., St Louis, E.K., Gregg, N.M., Lundstrom, B.N., Crowe, C.M., Attia, T.P., Crepeau, D., Balzekas, I., Marks, V.S., Wheeler, L.P., Cimbalnik, J., Cook, M., Janca, R., Sturges, B.K., Leyde, K., Miller, K.J., Van Gompel, J.J., Denison, T., Worrell, G.A. and Kremen, V. (2022) "Distributed brain co-processor for tracking spikes, seizures and behaviour during electrical brain stimulation," *Brain communications*, 4(3), p. fcac115. Available at: https://doi.org/10.1093/braincomms/fcac115.

Staniszewska, A., Mąka, A., Religioni, U. and Olejniczak, D. (2017) "Sleep disturbances among patients with epilepsy," *Neuropsychiatric disease and treatment*, 13, pp. 1797–1803. Available at: https://doi.org/10.2147/NDT.S136868.

Štillová, K., Jurák, P., Chládek, J., Chrastina, J., Halámek, J., Bočková, M., Goldemundová, S., Říha, I. and Rektor, I. (2015) "The role of anterior nuclei of the thalamus: A subcortical gate in memory processing: An intracerebral recording study," *PloS one*, 10(11), p. e0140778. Available at: https://doi.org/10.1371/journal.pone.0140778.

Sudhyadhom, A., Haq, I.U., Foote, K.D., Okun, M.S. and Bova, F.J. (2009) "A high resolution and high contrast MRI for differentiation of subcortical structures for DBS targeting: the Fast Gray Matter Acquisition T1 Inversion Recovery (FGATIR)," *NeuroImage*, 47 Suppl 2, pp. T44-52. Available at: https://doi.org/10.1016/j.neuroimage.2009.04.018.

Tellez-Zenteno, J.F., Patten, S.B., Jetté, N., Williams, J. and Wiebe, S. (2007) "Psychiatric comorbidity in epilepsy: a population-based analysis," *Epilepsia*, 48(12), pp. 2336–2344. Available at: https://doi.org/10.1111/j.1528-1167.2007.01222.x.

Van Gompel, J.J., Bower, M.R., Worrell, G.A., Stead, M., Meier, T.R., Goerss, S.J., Chang, S.-Y., Kim, I., Meyer, F.B., Richard Marsh, W., Marsh, M.P. and Lee, K.H. (2011) "Swine model for translational research of invasive intracranial monitoring: Swine Animal Model for Translational Intracranial EEG," *Epilepsia*, 52(6), pp. e49-53. Available at: https://doi.org/10.1111/j.1528-1167.2011.03096.x.

Vezzani, A., French, J., Bartfai, T. and Baram, T.Z. (2011) "The role of inflammation in epilepsy," *Nature reviews. Neurology*, 7(1), pp. 31–40. Available at: https://doi.org/10.1038/nrneurol.2010.178.

Vrinda, M., Arun, S., Srikumar, B.N., Kutty, B.M. and Shankaranarayana Rao, B.S. (2019) "Temporal lobe epilepsy-induced neurodegeneration and cognitive deficits: Implications for aging," *Journal of chemical neuroanatomy*, 95, pp. 146–153. Available at: https://doi.org/10.1016/j.jchemneu.2018.02.005.

Wang, Y.-C., Kremen, V., Brinkmann, B.H., Middlebrooks, E.H., Lundstrom, B.N., Grewal, S.S., Guragain, H., Wu, M.-H., Van Gompel, J.J., Klassen, B.T., Stead, M. and Worrell, G.A. (2020) "Probing circuit of Papez with stimulation of anterior nucleus of the thalamus and hippocampal evoked potentials," *Epilepsy research*, 159(106248), p. 106248. Available at: https://doi.org/10.1016/j.eplepsyres.2019.106248.

World Health Organization (2019) *Epilepsy: a public health imperative*. World Health Organization. Available at: https://apps.who.int/iris/bitstream/handle/10665/325293/9789241515931-chi.pdf.

Zhao, X., Liao, Y., Morgan, S., Mathur, R., Feustel, P., Mazurkiewicz, J., Qian, J., Chang, J., Mathern, G.W., Adamo, M.A., Ritaccio, A.L., Gruenthal, M., Zhu, X. and Huang, Y. (2018) "Noninflammatory changes of microglia are sufficient to cause epilepsy," *Cell reports*, 22(8), pp. 2080–2093. Available at: https://doi.org/10.1016/j.celrep.2018.02.004.

Zhu, F., Wang, H., Li, L., Bragin, A., Cao, D. and Cheng, Y. (2023) "Intracranial electrophysiological recordings on a swine model of mesial temporal lobe epilepsy," *Frontiers in neurology*, 14. Available at: https://www.frontiersin.org/articles/10.3389/fneur.2023.1077702.

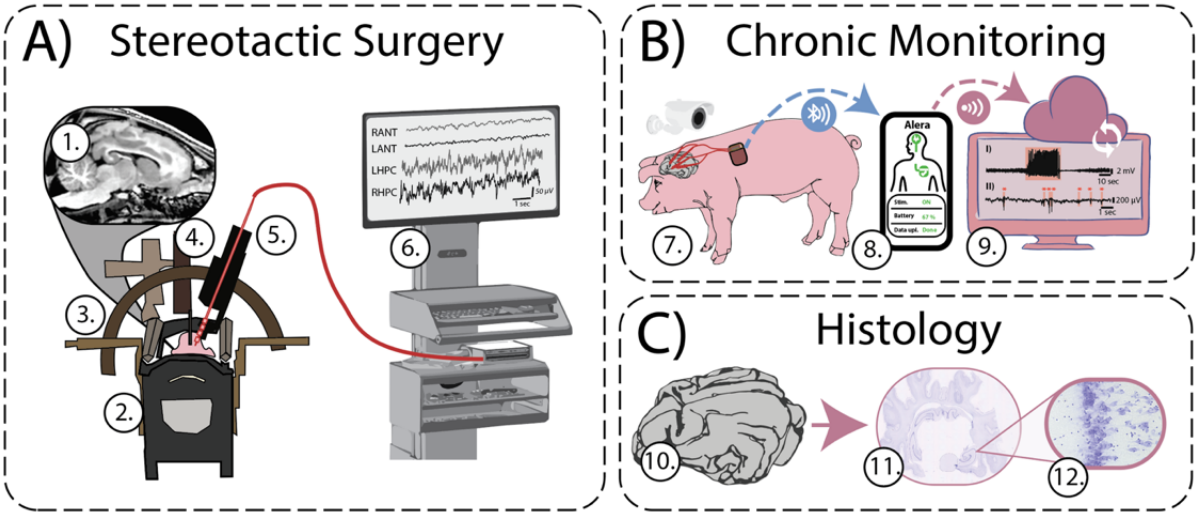

Figure 1: A Platform for Development of Chronic Large Animal Epilepsy Models. A) Stereotactic implantation surgery using 1) 3 Tesla pre-op MRI imaging, 2) Custom MRI compatible stereotactic frame for head fixation, 3) Stereotactic Leksell frame for electrode image compatible with Brainlab stereotactic planning software (Brainlab AG, Munich, Germany) , 4) Microinjector for kainic acid infusion and 5) Electrode delivery system to implant lead electrodes into bilateral ANT and HPC and inject KA into HPC. 6) Intra-operative workstation utilized to monitor brain LFP signals, perform single pulse electrical stimulation, and track the local field changes induced by KA infusion. **B) Chronic seizure monitoring** 7) Implanted animals were chronically monitored using a camera and an implantable four lead neural stimulating and recording device that wirelessly transfers LFP recordings using a Low Energy Bluetooth into 8) an Android phone application and 9) cloud with automated LFP signal processing for seizure and IED detection. **C) Brain Histology** was performed to investigate structural changes in the 10) explanted brains for 11) gross structural and 12) microscopic changes.

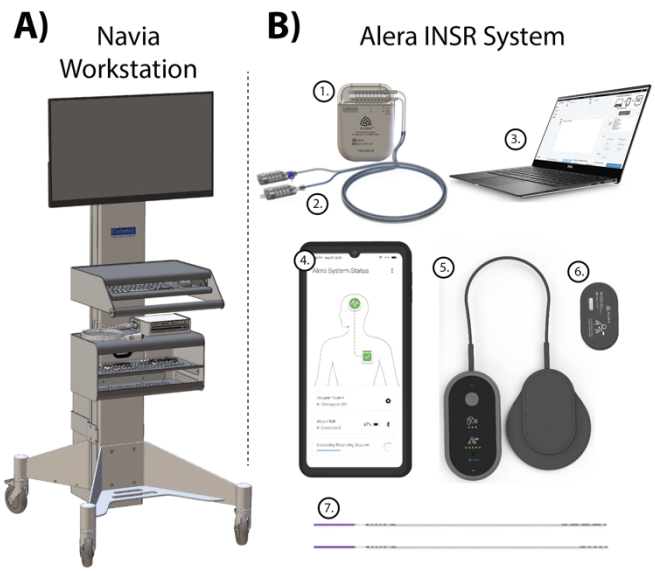

C) Technical Specifications

Sensing	Navia Workstation	Alera INSR
Sampling rate	8 kHz	8 kHz, 2 kHz, 500 Hz
Number of channels	16	16 (4 x 4 contacts)
Recording modes	Continuous	Continuous, Scanning
Input range	±0.7 V	±30 mV
Bandpass	0.1 Hz - 1 kHz	0.1 Hz - 1 kHz
Resolution	24 bit (100 nV)	16-bit (1.8 μV)
Memory	-	2 Gbit (nonvolatile)
Stimulation		
Type	Constant current	Constant current
Waveform	Biphasic, Charge-balanced	Biphasic, Charge-balanced
Compliance Voltage	±15 V	±12 V
Stimulation frequency	0.1 Hz to 166 Hz	0.1 Hz to 166 Hz
Pulse width	62.5 μs to 500 μs	62.5 μs to 500 μs
Resolution	0.1 mA to 20 mA	0.1 mA to 20 mA
Max Number of interleaved waveforms	8	8
Electrodes	**3.5 mm**	**7 mm**
Diameter	1.35 mm	1.35 mm
Tip length	2 mm	2 mm
Contact length	2 mm	2 mm
Contact spacing	1.5 mm	5 mm

Figure 2: Local Field Potential (LFP) Recording Instrumentation. A) Navia Workstation (NW) is a 16-channel recording, and stimulation platform. The NW enables high fidelity LFP sensing and recording (0.01 – 1000 Hz: Sampling 8 kHz) and programmable electrical stimulation. **B) Implantable Neural Stimulation and Recording (INSR) system Alera**. The INSR is a rechargeable, 16-channel sensing, stimulation and recording device. The Alera system includes: 1) 16 channel INSR supporting four leads with 2) electrode extensions with skull mounted bifurcation port, 3) programmer (Tablet computer), 4) controller (Android mobile phone), 5) charger, 6) control magnet and 7) electrode leads with 3.5 mm and 7 mm span were utilized within this study. The INSR can wirelessly communicate with the controller, relaying information such as the INSR battery level, operational status, and recording status; additionally, the controller may store recorded data downloaded from the INSR. The programmer is used to generate stimulation therapy programs that are uploaded to the INSR via the controller. **C) Detailed device specifications**.

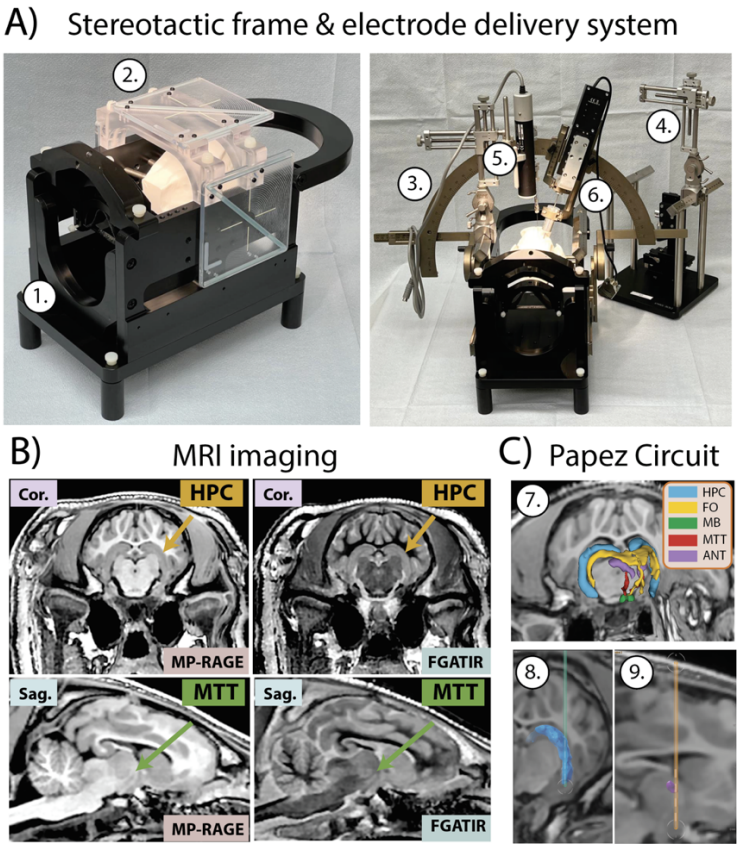

Figure 3: Stereotactic Electrode & KA Delivery. A) MRI compatible stereotactic frame. 1) A custom MRI compatible machined plastic head frame with jaw and skull set screws for head fixation (3D printed porcine skull) and 2) N-bar fiducial box compatible with Brainlab stereotactic software (Brainlab AG, Munich Germany). The frame is compatible with modified 3) Leksell arc-frame and 4) Kopf Instruments manipulator both providing 3 degrees of freedom for stereotactic targeting, 5) micro-injection delivery - UMP3 UltraMicroPump (World Precision Instruments, FL, USA) and 6) electrode lead implantation using a manual or computer-controlled electrode drive (w/o canula) for delivering electrode leads into the brain. **B) MRI scans utilized for pre-operative planning.** MPRAGE and FGATIR enable visualization hippocampus (HPC) and mammillothalamic tract (MTT) in coronal (Cor) and sagittal (Sag) slices. The MTT is utilized for direct visual targeting of the anterior nucleus of the thalamus (ANT). **C) Stereotactic Targeting of Papez Circuit** in the ANT and HPC. 7) Volumetric rendering of HPC, fornix (FO), mamillary bodies (MB), MTT and ANT for anatomy visualization in Slicer (Félix et al. 1999; Kikinis, Pieper, and Vosburgh 2014) and electrode plan for 8) HPC and 9) ANT leads.

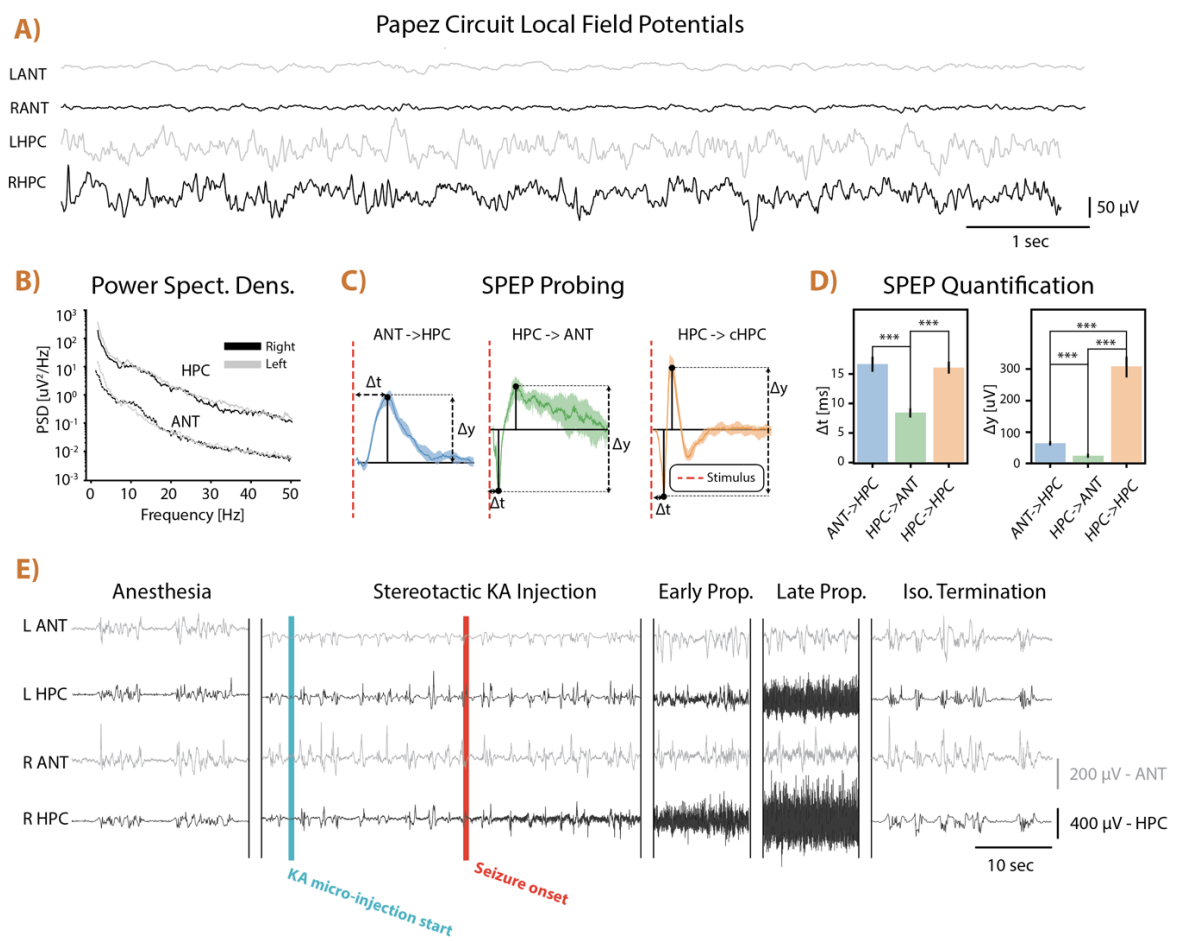

Figure 4. Intraoperative Electrophysiology of Papez Circuit and Acute Status Epilepticus
A) Representative intra-operative local field potential (LFP) traces from bilateral anterior nucleus of the thalamus (ANT) and hippocampus (HPC) under isoflurane anesthesia at baseline prior to hippocampal KA infusion. **B)** Power spectral density for ANT and HPC. The ANT LFPs are lower amplitude with decreased broadband power compared to HPC. **C)** Representative Single Pulse Evoked Potentials (SPEP) from ANT to HPC (ANT→HPC), HPC to ANT (HPC→ANT) and HPC to contralateral HPC (HPC→cHPC). **D)** The latency of initial negative response first peak (Δt) and peak to peak magnitude(Δy) were evaluated. D) Differences between ANT→HPC vs. HPC→ANT single pulse evoked potentials (SPEP) (Δt: 16.64 ± 5.88 ms vs 8.44 ± 2.25 ms, $p<10^{-6}$, Δy: 64.02 ± 33.13 µV vs 23.70±8.57 µV, $p<10^{-6}$). **E)** Baseline and post-KA infusion with recorded from HPC and ANT. Injection of KA provoked prolonged SE that was terminated after 20 minutes with Isoflurane. The onset of right (R) HPC seizure after KA infusion. The seizure propagates into the left (L) HPC and R ANT.

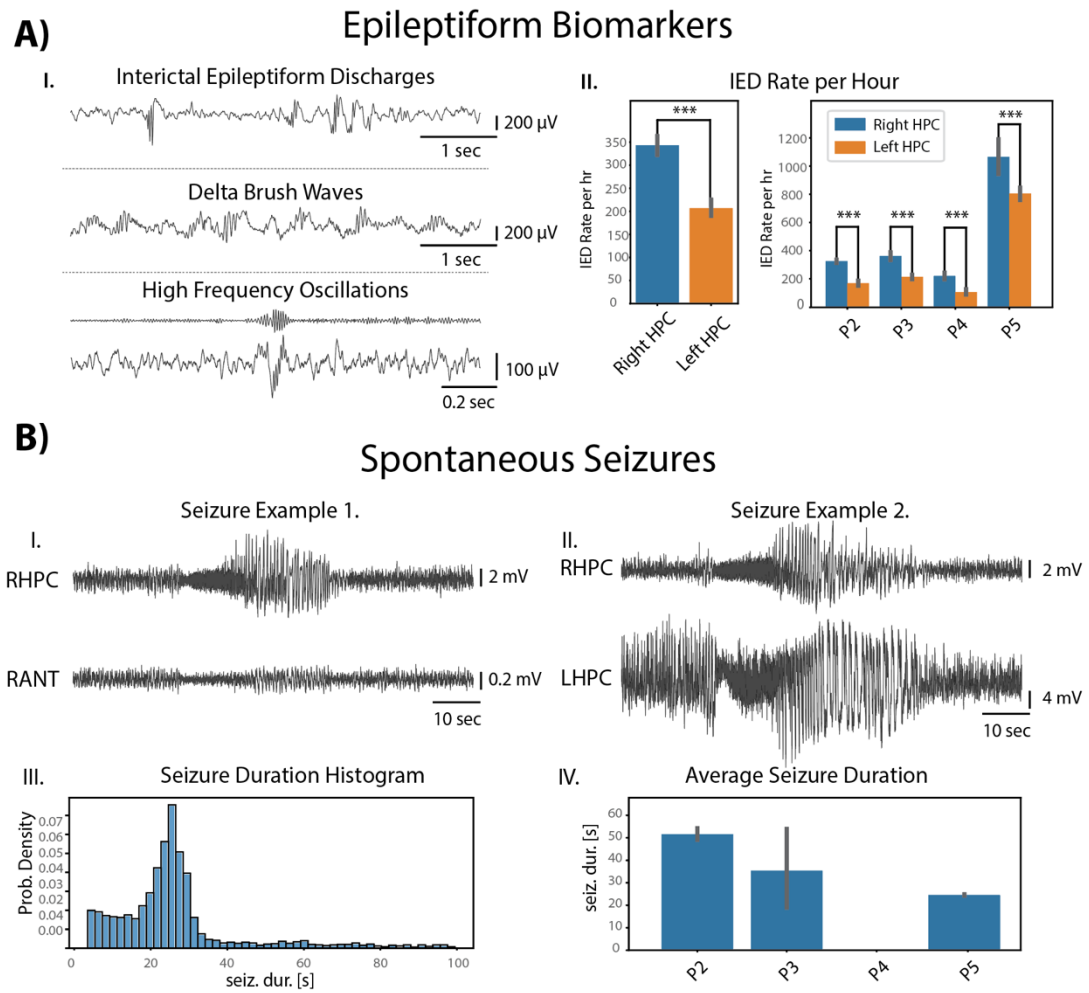

Figure 5. Spontaneous Interictal Epileptiform Discharges (IED) and Seizures in Chronic Pig Model.

A) Spontaneous IEDs during chronic INSR monitoring. ***I***. Representative example of IEDs, delta brush waveforms and high frequency oscillations (filtered between 80 Hz – 270 Hz). ***II***. IED rates in the left and right HPC, with higher hourly IED rate in the right HPC (KA site) compared to the contralateral HPC. **B) Spontaneous Seizures** during chronic INSR monitoring. ***I***. A representative right hippocampus (RHPC) seizure with recording from RHPC and right ant (RANT). ***II***. RHPC seizure without clear propagation into the right anterior nucleus of thalamus (RANT), compared to LHPC. ***III***. A histogram of automatically detected seizures. *IV*. A bar plot showing average seizure duration for each subject. Note, S4 did not have any seizure detections.

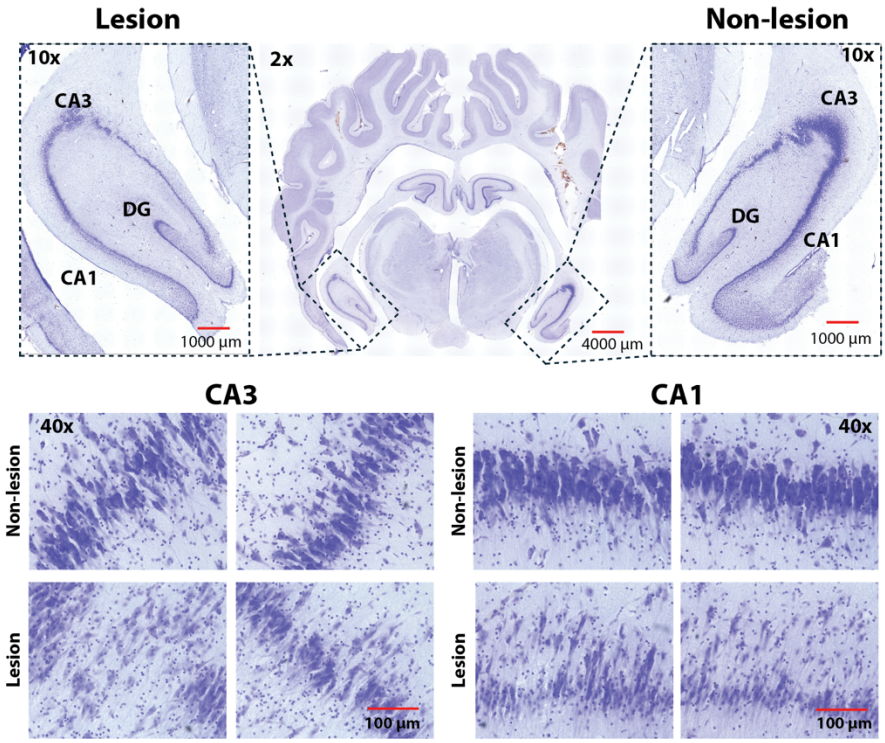

Fig. 6. Effect of intracerebral kainic acid (KA) administration on hippocampal cell death and organization in a porcine mTLE model. Coronal brain sections from four Yorkshire pig (Sus Scrofa) were processed by cresyl violet staining. Representative images at low (2x) magnification of the lesioned and contralateral (non-lesioned) hemispheres are shown. Boxed areas highlight the CA3, DG, and CA1 regions of the hippocampus at a higher (10x) magnification. Below (40x): Pyramidal cell disorganization and dispersion were predominant in the CA3 and CA1 lesioned region, compared to their contralateral control. Non-specific patches of pyramidal cell loss were observed in the pyramidal cell layer of the CA3 and in the CA1 region. Hippocampal regions are labeled for reference. CA1: Cornu Ammonis 1; DG: Dentate Gyrus; CA3: Cornu Ammonis 2; Hi: Hilus. Scale bars: 4000 µm at 2x, 1000 µm at 10x, 100 µm at 40x.

References

Félix, B., M. E. Léger, D. Albe-Fessard, J. C. Marcilloux, O. Rampin, and J. P. Laplace. 1999. "Stereotaxic Atlas of the Pig Brain." *Brain Research Bulletin* 49 (1–2): 1–137.

Kikinis, Ron, Steve D. Pieper, and Kirby G. Vosburgh. 2014. "3D Slicer: A Platform for Subject-Specific Image Analysis, Visualization, and Clinical Support." In *Intraoperative Imaging and Image-Guided Therapy*, 277–89. New York, NY: Springer New York.

Table 1: Six domestic Yorkshire pigs used for intrahippocampal Kainic Acid (KA) model. The weight at the time of implant; total injected KA dose; anesthesia (Anes) with isoflurane (I), Ketamine (K), Xylazine (X); hippocampal Interictal epileptiform discharges (IEDs), seizures, and status epilepticus (SE) (* - p<0.05; ** - p<0.01, *** p<0.001).

Subj.	Weight [kg]	KA Dose [µl]	Anest.	Maintained [days]	Spontaneous IEDs per Hour		Spontaneous Seizures			Events
					Left	Right	Seizures per day	Seizure duration [s]	Onset [days]	
S1	9.4	16	I	0	n/a	n/a	-	n/a	n/a	Euthanized with uncontrolled SE
S2	14.0	6	I	271	130.24 ± 201.87	**339.90±173.02 *****	19.32 ± 12.13	33.51 ± 27.73	9 days	SE, IED, SZ
S3	19.0	6	I	10	212.77 ± 56.04	**361.35±98.09 *****	6.00 ± 5.15	23.80 ± 25.07	7 days	SE, IED, SZ
S4	21.0	4	I	19	104.20 ± 201.59	**218.52±259.21 ****	-	-	-	SE, IED
S5	19.0	6	I, K, X	86	622.43 ± 295.11	607.39±590.62	107.20 ± 170.43	24.04 ± 9.08	15 days	SE, IED, SZ
S6	21.8	6	I, K, X	0	n/a	n/a	0	-	-	SE, IED, SZ Cardiopulmonary Arrest